Effects of Displacement History on Failure of Lightly Confined Bridge Columns

by R.T. Ranf, M.O. Eberhard, and J.F. Stanton

Synopsis: Six nominally identical reinforced concrete columns were subjected to a variety of lateral displacement histories to evaluate the effects of cycling on their failure displacement and failure mechanism. The columns, typical of bridges constructed before the mid-1970s, had circular cross-sections, low axial loads, and little transverse reinforcement. Shear failure caused five of the six columns to lose their axial load carrying ability at drift ratios between 3% and 5%. The sixth column failed in an axial-flexure mode at a drift ratio of 6%.

Increasing the number of cycles at each displacement level from one to fifteen decreased the maximum displacement preceding flexure-shear failure by approximately 35%. The effect of cycling on damage accumulation was modeled with the Park-Ang damage model, a Modified Park-Ang damage model, and a Cumulative Plastic Deformation damage model. The Cumulative Plastic Deformation model correlated best with the observed damage, and it was the easiest to implement.

R. Tyler Ranf, NSF Graduate Research Fellow, is a PhD student at the University of Washington. He received his BA in physics from the University of Puget Sound, his BS in civil engineering from Washington University in St. Louis in 2001, and his MSCE from the University of Washington in 2003.

Marc O. Eberhard, FACI, is a professor at the University of Washington. He received his BS in civil engineering, and materials science and engineering from the University of California, Berkeley, and his MSCE and Ph.D. from the University of Illinois. He chairs the seismic shear subcommittee of ACI-ASCE Committee 445, Shear and Torsion.

John F. Stanton, FACI, is a professor at the University of Washington. He holds a BA and MA from Cambridge (UK), an MSCE from Cornell and a PhD from the University of California, Berkeley. He is a member of ACI 318 E (Shear and Torsion), ACI 550 (precast Concrete) and ACI 554 (Joints and Bearings). His research interests include seismic behavior and design and prestressed concrete structures.

INTRODUCTION

The San Andreas fault and the Cascadia subduction zone have the potential for generating large-magnitude, long-duration earthquakes that might last several minutes (Heaton and Kanamori 1984, Kramer et al. 1998). Such long-duration earthquakes would impose numerous cycles of displacement on structures (Price 2000). Engineers need tools to evaluate the effects of this repeated cycling on damage accumulation in structures, especially in older reinforced concrete systems.

This paper discusses the effects of cycling on damage in laterally-loaded reinforced concrete columns typical of bridge construction of the 1950s, 1960s and early 1970s. Such columns usually have low axial loads and much less transverse reinforcement than is required in new bridges (Eberhard and Marsh 1997). The effect of cycling was investigated using three damage models: the Park-Ang damage model (Park and Ang 1985); a modified version of the Park-Ang model that does not require an estimate of the yield displacement; and the Cumulative Plastic Deformation damage model.

EXPERIMENTAL PROGRAM

This section describes the methodology followed to proportion the prototype column, the resulting test column properties, the testing setup, the instrumentation, and the testing procedure for the test columns. Ranf et al. (2005) provide details of the experiments.

Column prototype

The prototype was selected to be typical of circular bridge columns built before transverse reinforcement requirements increased following the 1971 San Fernando earthquake. Such older columns have suffered damage in many past earthquakes (Moehle and Eberhard 1999). Table 1 provides specifications and properties of typical

bridge columns built between the late 1940s and the early 1980s in Washington State (Ruth and Zhang 1999).

On the basis of the data provided in Table 1, the yield strength of the longitudinal and transverse reinforcement for the prototype column was chosen as 44 ksi (303 MPa), 10% larger than the specified minimum for columns built before 1977. The concrete strength for the prototype was chosen as 6000 psi (41.4 MPa), 50% larger than the specified minimum for columns presented in Table 1. This increase reflects the effects of long-term strength gain and of the difference between the expected mean and specified strengths (Priestley et al 1992).

The prototype geometry was based on the results of a survey by Ruth and Zhang (1999) of 33 bridges in Washington State that were built between 1957 and 1969. They found that the diameter of 212 of the 216 columns (98%) in these bridges was between 4 and 6 feet (1219 and 1829 mm), with approximately half of these columns having a diameter of 5 feet (1524 mm). The lengths of the majority of columns ranged from 20 to 25 feet (6096 to 7620 mm). Assuming that the distance between the footing and the inflection point is slightly larger than half the column length, these fixed columns have cantilever lengths of about 15 feet (4572 mm) and an aspect ratio of 3. The transverse reinforcement for the surveyed columns consisted nearly always of #4 hoops at 12 in. (305 mm) spacing, independent of the column diameter.

Based on these findings, the prototype column was chosen to be 5 feet in diameter with #4 hoops spaced at 12 in. (305 mm) and an overlap of 24 in. (610 mm). The minimum cover to the outside of the hoop was chosen to be 1.5 in. (38.1 mm), resulting in a volumetric ratio for the transverse reinforcement of 0.12%. This value is far below the current transverse reinforcement requirements of at least 0.56% in non-seismic applications and 1.2% in seismic applications (AASHTO 2004). The longitudinal reinforcement ratio ($\rho_l = A_s/A_g$, where A_s and A_g are the areas of the longitudinal steel and column cross-section) was assumed to be 1.0%, because this value is common in practice. The axial-load ratio ($P/A_g f'_c$, where P and f'_c are the axial load and the concrete compressive strength) was selected as 10%. This value is at the high end of the range for bridge columns in practice.

Test columns

The test columns were designed to be 1/3 the size of the prototype, resulting in a model column height and diameter of 5 feet (1524 mm) and 20 in. (508 mm), respectively. The geometry and reinforcement of the test columns are shown in Fig. 1. Table 2 compares key properties of the prototype and test columns.

The material properties of longitudinal and transverse reinforcement are listed in Table 3. Reinforcing bars with a yield strength of 44 ksi (303 MPa) were not available, so ten D16 grade 420 bars were used as the longitudinal reinforcement. This choice preserved the reinforcement ratio and the scaling for bar size, but resulted in a tension strength that was approximately 50% greater than that of the prototype. Concrete cover and maximum aggregate size were scaled to the nearest available dimension.

The transverse reinforcement for the prototype columns was #4 bars at 12 in. (305 mm) centers with f_y = 44 ksi (303 MPa). Scaling all features of the ties was not possible, so instead, the transverse reinforcement was modeled with W2.5 smooth wire hoops at 4 in. (102 mm) centers. With this arrangement, the hoop spacing, transverse bar diameter and transverse reinforcement ratio were scaled to within 15% of their ideal values. However, because this material has a yield strength, f_y, of 80 ksi (552 MPa), the tension strength per bar was twice its ideal value. Furthermore, W2.5 wire was only available in smooth wire, which would be expected to have weaker bond properties than those of a #4 deformed bar.

The six test specimens were cast in four pours, (two for the footings, and two for the columns and hammerheads). Concrete cylinders were stored in the laboratory fog room until they were tested. The compressive strength, f'_c, split cylinder tensile strength, f_{ct}, and elastic modulus, E_c, for each concrete batch are reported in Table 4. Nearly all tests for the material properties were conducted within two days of column testing. However, the elastic modulus for column S1 was determined on the day of testing for column S15. Additionally, the compression tests for column C3R were conducted approximately three weeks after testing.

The average concrete compressive strength of the first four columns tested (S3, C2, C4 and C3R) was 8050 psi (55.5 MPa), 34% larger than the target 56-day strength of 6000 psi (41.4 MPa). This discrepancy can be partly attributed to the average age at testing of the specimens in the group of 192 days. The average strength of the last two columns (S1 and S15) was 5570 psi (38.4 MPa), which was closer to the target value of 6000 psi (41.4 MPa). The strength of the concrete in the footings was nearly 30% higher for S1 and S15 (average of 6360 psi) than for the other four columns (average of 4980 psi).

Test setup

The testing apparatus was designed to maintain a constant axial load while subjecting the column to transverse cyclic displacements (Fig. 2). An axial load of approximately $0.1f'_cA_g$ was applied to each column through a steel cross-head placed on a spherical bearing on the column hammerhead, stressed to the floor by two high-strength rods. The transverse load was applied to the hammerhead using a servo-controlled actuator. The column footing was anchored to the floor using two high-strength rods, each stressed to 125 kips (556 kN).

Instrumentation

The instrumentation scheme is shown in Fig. 3. Axial and lateral forces were measured using load cells. Transverse displacements were measured using five potentiometers at various heights up the column, with two more at the base to monitor footing slip.

Reinforcement strains and relative cross-sectional rotations were measured in columns S3, C2, C4 and C3R, but not in S1 and S15. Eight strain gauges were placed on each of the two longitudinal bars that were nearest to the front and back faces of the column (bars

A and C in Fig. 3). One gauge was also placed on the two longitudinal bars that were nearest to the column sides (bars B and D in Fig. 3). The transverse reinforcement was instrumented with strain gauges at four elevations: 2, 6, 10 and 18 inches (51, 152, 254 and 457 mm) above the top of the footing.

Testing procedure

The naming convention for the columns, provided in Table 5, was based on the characteristics of the imposed displacement histories (Table 6). The histories were chosen to provide a wide range of displacement paths with which to calibrate damage models.

The displacement histories were based on a sequence of nine drift ratios, ranging from 0.27% to 5.72%, each being approximately 1.5 times the previous one. Two series of displacement histories were applied to the columns ("C" and "S"). The main portion of the displacement history for columns C2, C3R and C4 consisted of at least 10 cycles of displacement amplitude at drift ratios of approximately 2%, 3% and 4%, respectively. Column C3R had the additional "R" designation, because after cycles were applied at a drift ratio of 3%, the level of displacement was reduced to a drift ratio of 2%

The S test series consisted of "standard" displacement history, in which the displacement amplitudes increased consistently throughout the test, although at different rates. Columns S1 and S3 were subjected respectively to 1 and 3 cycles at each of the standard drift ratios. The S3 loading therefore resembles closely a loading pattern used by many researchers in the past (e.g., Lehman et al, 2004). Column S15 was subjected to 15 cycles between each standard drift ratio in such a way that the amplitude of each half cycle was a constant multiple of the previous one. This unusual displacement history was developed in order to achieve large values for dissipated energy and accumulated plastic strain while increasing the maximum displacement very gradually. Separating energy from maximum displacement in this way is necessary for evaluating the relative importance of the components of damage models. The damage models are discussed later in this paper.

FORCE-DISPLACEMENT RESPONSE

The effective force-displacement histories for each column are shown in Fig. 4. The effective force is equal to the maximum column moment divided by the length of the cantilever column. It includes the effect of both lateral and vertical loads. The drift ratio is given by the transverse column displacement divided by the cantilever column length.

The variations in the maximum effective forces of the six test columns are primarily attributable to variations in the material properties and axial load. For example, because the concrete strengths for columns S1 and S15 were lower than those for columns S3, C2, C4 and C3R, the axial load was also smaller to maintain the same axial-load ratio. Ranf et al. (2005) showed that the measured flexural strength of the columns can be reproduced accurately with moment-curvature analyses. The ratio of the measured

maximum moment to the calculated maximum moment for the six columns had a mean of 1.1 and a coefficient of variation of 5.1% (Ranf et al. 2005).

Fig. 5 shows the axial load-horizontal displacement history for each column. The target axial-load ratio for each test was 10%. The axial load varied significantly with the horizontal displacement for columns S1, S3, and C4, but the maximum load applied to the columns never exceeded 15% of $A_g f_c'$. The axial load was adjusted continuously for columns S15, C2 and C3R.

The yield displacement of each column was determined experimentally using two methods. For columns with strain gauges (columns S3, C2, C4 and C3R), the initial yield displacement was determined from the point at which the first strain gauge at the column base reached the yield strain of the longitudinal reinforcement. For all six columns, the initial yield displacement was also obtained from the measured force-displacement envelope based on the moment at initial yield, M'_y. Table 7 shows that the yield displacements calculated with both methods were similar for the four columns in which both measurements were available.

Table 7 also shows that the yield displacements are clustered into two groups: columns S1 and S15 had an average Δ_y of 0.26 in. (6.48 mm), whereas columns S3, C2, C4, and C3R had an average Δ_y of 0.37 in. (9.27 mm). The difference between these two groups was attributed to additional anchorage slip caused by the presence of strain gauges in the footings of columns S3, C2, C4 and C3R; and to the higher strength and elastic modulus of the footing concrete in S1 and S15.

INFLUENCE OF CYCLING ON DAMAGE ACCUMULATION

All of the columns yielded in flexure, spalled at their bases, and experienced buckling of the longitudinal bars before shear damage was observed. This behavior was consistent with the flexural damage model developed by Berry and Eberhard (2003), which estimated the onset of spalling and bar buckling at drift ratios of 1.87% and 4.00%, respectively. Table 8 shows the maximum column displacement, the hysteretic energy dissipated, and the cumulative plastic deformation for each column at 20% and 50% loss of flexural strength and at loss of axial load.

Fig. 6 shows the effect of cycling on the maximum displacement at 20% loss of flexural strength. The drift ratio for this damage state decreased as cycling increased, regardless of whether cycling was quantified in terms of dissipated energy or cumulative plastic deformation. In contrast, no trends were apparent when the maximum displacement was quantified in terms of the displacement ductility, because the yield displacement varied among the columns (Table 7). Ranf et al. (2005) show that the trends were similar for 50% strength loss.

All of the columns eventually lost their ability to carry the imposed axial load (Fig. 5). The effect of cycling on loss of axial-load carrying capacity is shown in Fig. 7. As with the other damage states, cycling tended to decrease the displacement at failure. The

exception was column C4 (the only column to have an axial-flexure failure), which failed at a higher drift ratio (6%) than any of the other columns. Five of the six columns had a shear-flexure failure mode, in which a large diagonal crack formed within the hinge region at the base of the columns (Fig. 8a). The sixth column failed in an axial-flexure mode, without the formation of a diagonal crack (Fig. 8b).

CALIBRATION OF DAMAGE MODELS

The effect of cycling on damage accumulation in each column was characterized using three damage models. The Park-Ang damage model (Eq. 1) is the method most commonly used for characterizing the effect of cycling on damage.

$$D = \alpha \frac{\Delta_{max}}{\Delta_y} + \beta \frac{E_h}{\Delta_y F_y} \tag{1}$$

in which D is the damage index level, Δ_{max} is the maximum displacement experienced by the structure, Δ_y is the yield displacement, E_h is the hysteretic energy dissipated during cycling, F_y is the force at yield. The dimensionless coefficients α and β are obtained by calibration against measured test data. To estimate E_h, it is necessary to know (or estimate) a column's cyclic force-displacement history, because this parameter is sensitive to the shape of the hysteresis loops. The Park-Ang model is also sensitive to the accuracy of the estimation of the yield displacement, which appears in the denominator of both terms. As mentioned previously, the yield displacements of columns S1 and S15 were significantly smaller than the yield displacements of the other four columns (Table 7).

To reduce the model's sensitivity to the yield displacement, a Modified Park-Ang model was investigated, which normalizes the data by the column length, L, instead of the yield displacement. This model is given by the equation

$$D = \alpha_m \frac{\Delta_{max}}{L} + \beta_m \frac{E_h}{L F_y} \tag{2}$$

where α_m and β_m are dimensionless coefficients.

A third model, called the Cumulative Plastic Deformation damage model, was developed to characterize the effects of cycling through the total amount of plastic deformation experienced by the column, and is given by.

$$D = \alpha_p \frac{\Delta_{max}}{L} + \beta_p \frac{\Sigma\Delta_p}{L} \tag{3}$$

where α_p and β_p are dimensionless coefficients. This model can be implemented on the basis of a column's displacement history, without needing to estimate the force history. Also, the value of $\Sigma\Delta_p$ is insensitive to the shapes of the hysteresis loops.

Each of the damage models was calibrated using a least squares best-fit approximation of the data shown in Table 8. Because column C4 eventually experienced a flexural failure, as opposed to flexure-shear failures of the other five columns, the damage models at the loss of axial load damage state were calibrated both with and without the data from column C4. Figs. 6 and 7 show these best-fit lines, and illustrate that because the data for columns S1, S3, C2, C4 and C3R are clustered together, the least squares fit depends heavily on the data for column S15.

The damage model coefficients for each damage model (α and β in Eq. 1, α_m and β_m in Eq. 2, and α_p and β_p in Eq. 3), and the correlation coefficient (R^2) for the best-fit lines are provided in Table 9 for each damage state. The correlation coefficients are extremely low for the Park-Ang model. This is due to the variation in the values of measured yield displacements of the nominally identical columns. The correlation coefficients for both the Modified Park-Ang damage model and the Cumulative Plastic Deformation damage model are similar for each damage state, particularly at 20% and 50% loss of lateral load. The correlation coefficient was the highest ($R^2 = 0.68$) for the Cumulative Plastic Deformation damage model for the loss-of-axial-load damage state.

SUMMARY AND CONCLUSIONS

Six columns were subjected to a variety of displacement histories to evaluate the effects of cycling on the failure displacement and mechanism of lightly confined reinforced concrete columns. Damage accumulation was evaluated for three levels of column damage: 20% loss of flexural strength, 50% loss of flexural strength, and loss of axial-load carrying capacity. Cycling reduced the displacement at which the flexural strength of the columns decreased (20% or 50%) and when the columns lost their ability to carry the imposed axial load. For example, the maximum displacement preceding flexure-shear failure decreased by 35% when the number of cycles at each displacement level was increased from one to fifteen.

Three damage models were used to characterize the effect of cycling on damage accumulation. The Park-Ang (1985) damage model accounts for cycling in terms of the dissipated hysteretic energy, and it normalizes this data by the yield force and yield displacement. Although the six columns were nominally the same, the measured yield displacements of columns S1 and S15 were significantly smaller than the yield displacements of columns S3, C2, C4 and C3R. Consequently, the Park-Ang damage index, which is sensitive to the estimate of the yield displacement, correlated poorly with the observed damage.

The Modified Park-Ang damage model normalized the displacement demands by the yield force and column length. Although this model reduced the sensitivity of the model to the variations in estimated yield displacement, it was still necessary to estimate the cyclic, force-displacement response to compute dissipated hysteretic energy.

The Cumulative Plastic Deformation damage model quantifies cycling as the summation of the column displacement beyond yield, and normalizes these data by the column

length. Although it is still necessary to estimate the yield displacement, this model is relatively insensitive to inaccuracies in the estimate of the yield displacement. Of the three damage models studied, the Cumulative Plastic Deformation model yielded the best correlation coefficient (highest R^2). This measure has the additional advantage that it can be computed without estimating the force-displacement history for the column. The Cumulative Plastic Deformation damage model is the most effective method for characterizing the effect of cycling on a column's shear strength, because it fit the data best, and it was the easiest to implement.

ACKNOWLEDGEMENTS

REFERENCES

AASHO (1953), *Standard Specifications for Highway Bridges (6th Edition)*. The American Association of State Highway Officials (AASHO), Washington, D.C.

AASHO (1961), *Standard Specifications for Highway Bridges (8th Edition)*. The American Association of State Highway Officials (AASHO), Washington, D.C.

AASHO (1965), *Standard Specifications for Highway Bridges (9th Edition)*. The American Association of State Highway Officials (AASHO), Washington, D.C.

AASHTO (1989), *Standard Specifications for Highway Bridges (14th Edition)*. The American Association of State Highway and Transportation Officials (AASHTO), Washington, D.C.

AASHTO (2004), *LRFD Bridge Design Specifications (3rd Edition)*. The American Association of State Highway and Transportation Officials (AASHTO), Washington, D.C.

Berry, M. and Eberhard, M. (2003), "Performance Models for Flexural Damage in Reinforced Concrete Columns," Report No. 2003/18, Pacific Earthquake Engineering Research Center.

Eberhard, M.O. and Marsh, M.L., (1997), "Lateral-Load Response of two Reinforced Concrete Bents." *Journal of Structural Engineering*, American Society of Civil Engineers (Structural Division), 123(4).

Heaton, T.H., Kanamori, H., (1984), "Seismic Potential Associated with Subduction in the Northwestern United States," *Bulletin of the Seismological Society of America*, 74(3), 933-941.

Kramer, S. L., Silva, W. J., Baska, D. A., (1998), "Ground Motions Due to Large Magnitude Subduction Zone Earthquakes." *Technical Report WA-RD 450.1*. Washington State Transportation Center.

Lehman, D., Moehle, J., Mahin, S., Calderone, A., and Henry, L. (2004), "Experimental Evaluation of the Seismic Performance of Reinforced Concrete Bridge Columns," Journal of Structural Engineering, American Society of Civil Engineers (Structural Division) 130(6), 869-879.

Moehle, J.P. and Eberhard, M.O. (1999), "Earthquake Damage to Bridges," Chapter 34 in The Handbook of Bridge Engineering, Ed. W.F. Chen and L. Duan, CRC Press, 34.1-34.33.

Mookerjee, A. (1999), *Reliability of Performance Estimates of Spiral and Hoop Reinforced Concrete Columns*. Master's Thesis, Department of Civil Engineering, University of Washington, Seattle, Washington.

Park, Y.-J., and Ang, A.H.-S. (1985), "Mechanistic Seismic Damage Model." *Journal of Structural Engineering*, American Society of Civil Engineers (Structural Division), 111(4), 722-739.

Price, Z.M. (2000), *Bridge Column Damage Estimates for Cascadia Subduction Zone Earthquakes*. Master's Thesis, Department of Civil and Environmental Engineering, University of Washington, Seattle, Washington.

Priestley, M.J.N., Seible, F., and Chai, Y.H. (1992),"Design Guidelines for Assessment, Retrofit and Repair of Bridges for Seismic Performance," Rep. No. SSRP-92-01, Dept. of Applied Mechanics and Engineering Science, University of California, San Diego, California.

Ranf, R.T., Nelson, J.M., Price, Z., Eberhard, M.O., and Stanton, J.F. (2005). "Damage Accumulation in Lightly Confined Reinforced Concrete Bridge Columns" Report No. 2005/08, Pacific Earthquake Engineering Research Center.

Ruth, C., and Zhang, H. (1999), Personal Correspondence. Washington State Department of Transportation (WSDOT), Olympia, Washington.

WSDOT (September 1993), *Bridge Design Manual (M23-50)*.   Washington State Department of Transportation (WSDOT), Olympia, Washington.

NOTATION

A_g – Column cross-sectional area
A_s – Total area of longitudinal reinforcement
D – Damage index
E_c – Elastic modulus of concrete
E_h – Hysteretic energy dissipated
F_y – Column yield strength
f'_c – Concrete strength
f_{ct} – Concrete tensile strength
f_y – Yield stress of steel
L – Column length
M'_y – Column moment at initial yield
P – Axial load

α – parameter for Park-Ang damage model
α_m – parameter for Modified Park-Ang damage model
α_p – parameter for Cumulative Plastic Deformation damage model
β – parameter for Park-Ang damage model
β_m – parameter for Modified Park-Ang damage model
β_p – parameter for Cumulative Plastic Deformation damage model
Δ – Column displacement
Δ_{max} – Maximum column displacement
Δ_y – Column yield displacement
ε_y – Yield strain of longitudinal steel
ρ_l – Longitudinal reinforcement ratio
ρ_t – Transverse reinforcement ratio

Table 1 – WSDOT specifications for bridge columns (Ruth and Zhang 1999)

Specifications Year	Concrete		Reinforcing Steel		
	Class	f'_c (psi)	Longitudinal f_y (ksi)	Transverse f_y (ksi)	Comment
1948	A	3600	40	40	ASTM A15, Intermediate Grade
1951 (1948 Amend. 1)	A	3600	40	40	ASTM A15, Intermediate Grade
1953 (1948 Amend. 2)	A	3600	40	40	ASTM A15, Intermediate Grade
1957	A	3600	40	40	ASTM A15, Intermediate Grade
1963	AX	4000	40	40	ASTM A15, Intermediate Grade
1966 (1963 Amend. 1)	AX	4000	40	40	ASTM A15, Intermediate Grade
1968(1963 Amend. 2)	AX	4000	40	40	ASTM A15, Intermediate Grade
1969	AX	4000	40[1]	40[2]	[1] ASTM A615, Grade per plans [2] ASTM A615, Grade 40
1972	AX	4000	40	40	ASTM A615, Grade 40 except as noted on plans
1974	AX	4000	40	40	ASTM A615, Grade 40 except as noted on plans
1977	AX	4000	60[1]	60[2]	[1] ASTM A615, Grade 60 except as noted on plans [2] Spiral tie. ASTM A615, plain bar Grade per plans
1980	AX	4000	60[1]	60[2]	[1] ASTM A615, Grade 60 except as noted on plans [2] Spiral tie. ASTM A615, plain bar Grade per plans

Table 2 – Details of prototype and test columns

Item	Prototype	Test Column	Remarks
Column Length	15 feet	5 feet	1:3 Scale
Column Diameter	60 in.	20 in.	1:3 Scale
Longitudinal Steel Ratio	$\rho_l = 1.0\%$	$\rho_l = 0.99\%$	Conserved during scaling
Transverse Hoops	No. 4 Grade 40 @ 12-in. spacings	W2.5 wire @ 4-in. spacings	1:3 scale on spacing
Transverse Reinforcement Ratio	$\rho_t = 0.12\%$	$\rho_t = 0.15\%$	Far below current requirements
Cover to Hoop	1.5 in.	0.57 in.	1:2.6 Scale
Concrete Compressive Strength	6000 psi	6000 psi	Target properties
Axial Load	$0.10f'_cA_g$	$0.10f'_cA_g$	f'_c = actual concrete strength
Maximum Aggregate Size	1 in.	3/8 in.	1:2.7 Scale

Table 3 – Reinforcing steel properties

Property	Longitudinal Steel	Transverse Steel
Average Yield Strength (f_y)	66 ksi (455 MPa)	60 ksi (414 MPa)
Average Ultimate Strength (f_u)	105 ksi (724 MPa)	66 ksi (455 MPa)

Table 4 – Concrete properties near time of testing

Column Name	Age at Test (days)	Column			Footing		
		f_c' (psi)	f_{ct} (psi)	E_c (ksi)	f_c' (psi)	f_{ct} (psi)	E_c (ksi)
S1	16	5270	520	4720	6320	---	5480
S3	159	8150	630	4090	4910	470	3260
S15	26	5870	550	4720	6390	580	5480
C2	199	8260	620	4270	4920	370	3610
C4	188	8170	540	4040	5010	430	3280
C3R	220	7640	600	4930	5080	430	3530

Table 5 – Test column names and description

Column Name	Description
S1	1 standard cycle between each displacement level, with the displacement incremented each half cycle, until failure
S3	3 standard cycles at each displacement level until failure
S15	15 standard cycles between each displacement level, with the displacement incremented each half cycle, until failure
C2	Constant amplitude cycling at a drift ratio of 2%
C4	Constant amplitude cycling at a drift ratio of 4%
C3R	Constant amplitude cycling at a drift ratio of 3%, followed by a decrease in the amplitude of cycling.

Table 6 – Summary of column displacement histories

Drift Ratio (%)	Cycle Numbers at Each Drift Level					
	Column S1	Column S3	Column S15	Column C2	Column C4	Column C3R
0.04		1				
0.07		2-4		1	1	1
0.27	1	5-7	1-15			
0.48	2	8-10	16-30			
0.77	3	11-13	31-45	2	2	2
1.15	4	14-16	46-60			
1.90	5	17-19	61-75	3-14		13-17
3.05	6	20-22		15-17		3-12
3.82				18	3-12	
4.57		23				
5.72					13	

Table 7 – Comparison of strain gauge and force-displacement data

Column	Based on $\varepsilon = \varepsilon_y$		Based on $M_{base} = M'_y$		
	Δ'_y (in.)	Δ_y (in.)	Δ'_y (in.)	Δ_y (in.)	F_y (k)
S1	---	---	0.22	0.26	44.3
S3	0.33	0.39	0.32	0.38	58.8
S15	---	---	0.19	0.23	46.5
C2	0.29	0.35	0.30	0.36	57.2
C4	0.37	0.44	0.29	0.35	57.1
C3R	0.37	0.44	0.31	0.37	56.8
Note: Strain gauges were not installed in columns S1 and S15					

Table 8 – Measured displacement capacities

Column	20% loss of flexural strength			50% loss of flexural strength			Loss of axial load		
	Δ_{max} (in.)	E_h (k-in.)	$\Sigma\Delta_p$ (in.)	Δ_{max} (in.)	E_h (k-in.)	$\Sigma\Delta_p$ (in.)	Δ_{max} (in.)	E_h (k-in.)	$\Sigma\Delta_p$ (in.)
S1	2.27	269	15.3	2.34	272	15.4	2.73	381	26.8
S3	2.12	640	33.2	2.12	639	33.2	2.85	709	41.1
S15	1.62	1120	115	1.66	1180	121	1.76	1190	124
C2	2.25	806	57.1	2.28	907	60.6	2.25	929	63.2
C4	2.23	231	5.88	2.29	614	40.5	3.54	852	80.2
C3R	1.78	502	29.1	1.80	745	51.2	1.80	854	69.2
μ	2.05	595	42.6	2.08	726	53.7	2.49	819	67.4
σ	0.28	338	39.5	0.29	305	36.5	0.69	267	33.8
δ (%)	14	57	93	14	42	68	28	33	50

Table 9 – Damage model parameters

| Damage Model	Model Parameters	Damage Level			
		20% loss of flexural strength	50% loss of flexural strength	Loss of axial load (including column C4)	Loss of axial load (excluding column C4)
Park-Ang	$1/\alpha$	6.20	6.39	8.19	7.49
	$1/\beta$	-898	-1440	1140	3220
	R^2	0.02	0.03	0.01	0.00
Modified Park-Ang	$1/\alpha_m$	3.91	4.21	5.85	5.42
	$1/\beta_m$	1.48	1.30	0.89	0.87
	R^2	0.43	0.48	0.30	0.55
Cumulative Plastic Deformation	$1/\alpha_p$	3.75	4.00	5.09	5.05
	$1/\beta_p$	775	670	612	438
	R^2	0.47	0.50	0.68	0.66
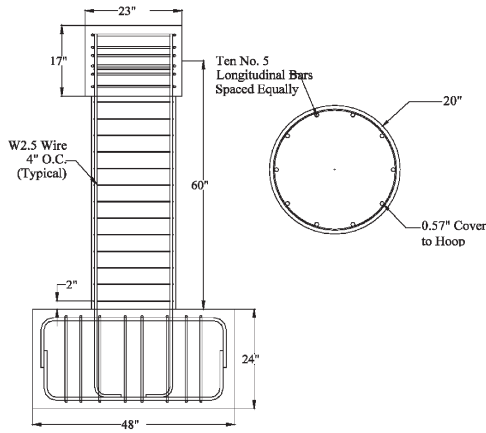
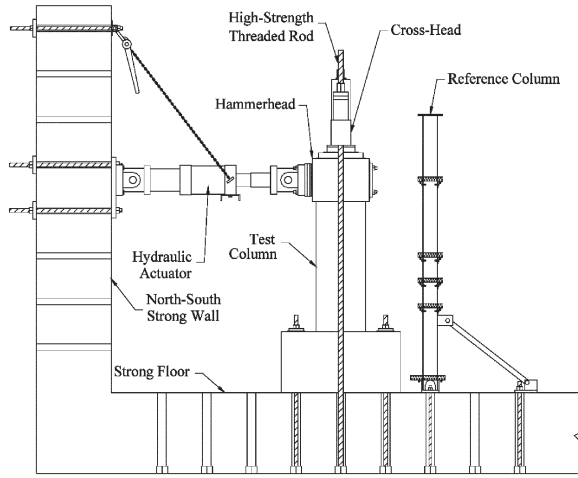Figure 1 – Test column geometry and reinforcement.

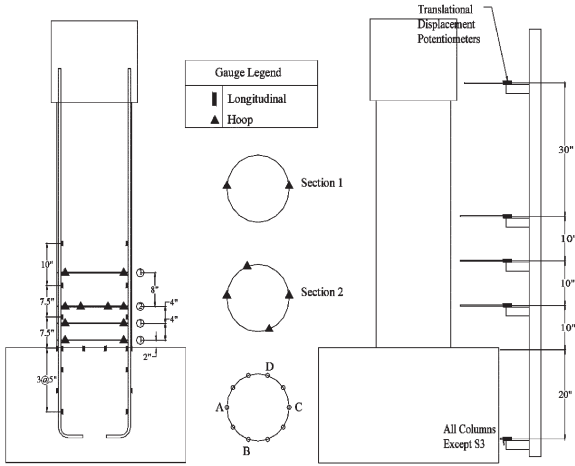Figure 2 – Testing apparatus.

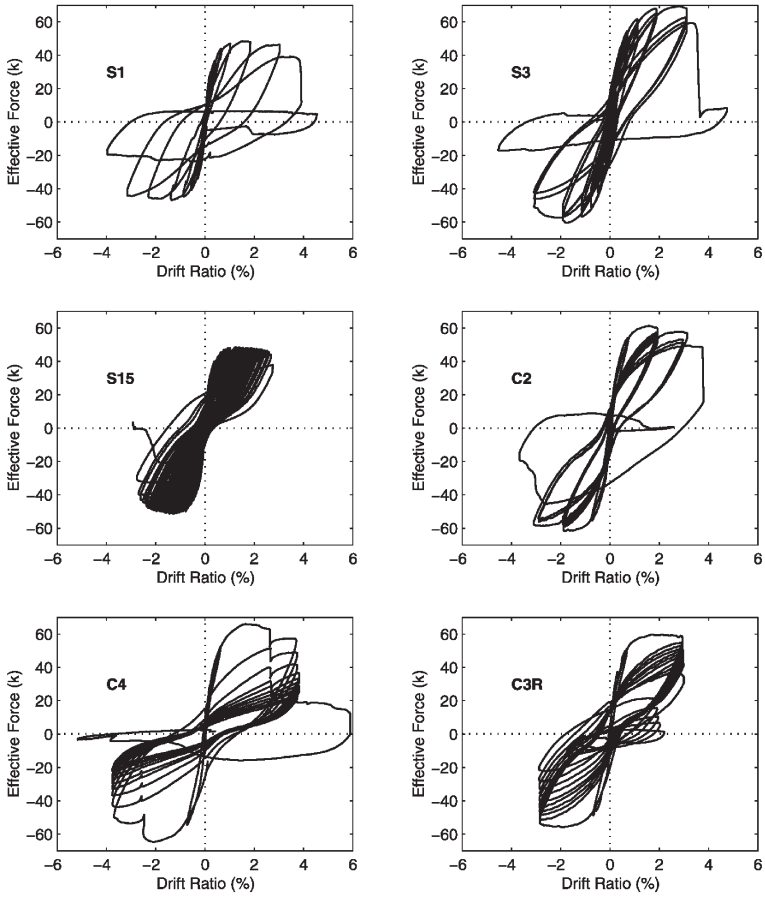Figure 3 – Column instrumentation.

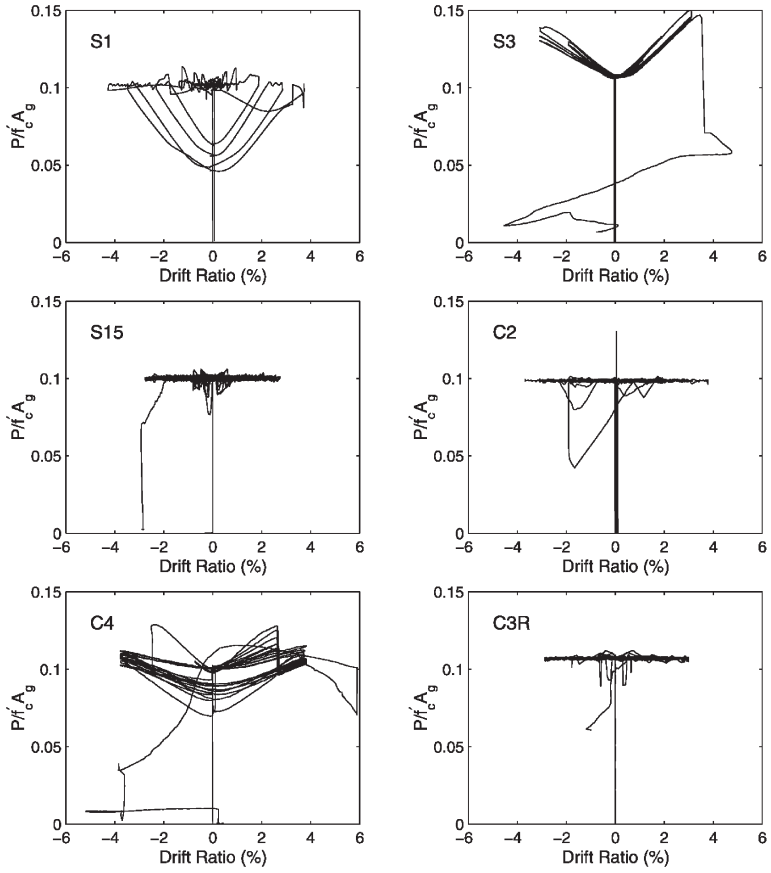Figure 4 – Effective force – displacement histories.

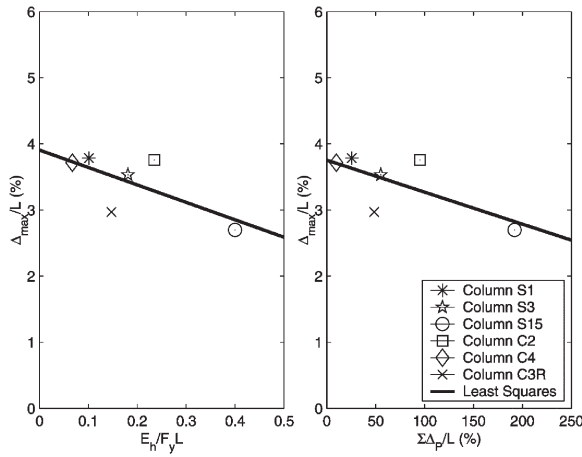Figure 5 – Axial load versus horizontal displacement histories.

Figure 6 – Drift ratios at 20% loss of flexural strength for the: (a) modified Park-Ang; and (b) cumulative plastic deformation damage models.
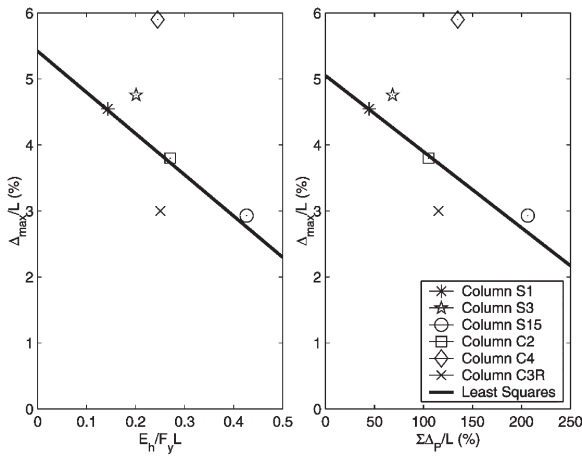

Figure 7 – Drift ratios at loss of axial load for the: (a) modified Park-Ang; and (b) cumulative plastic deformation damage models (calibration excludes column C4).
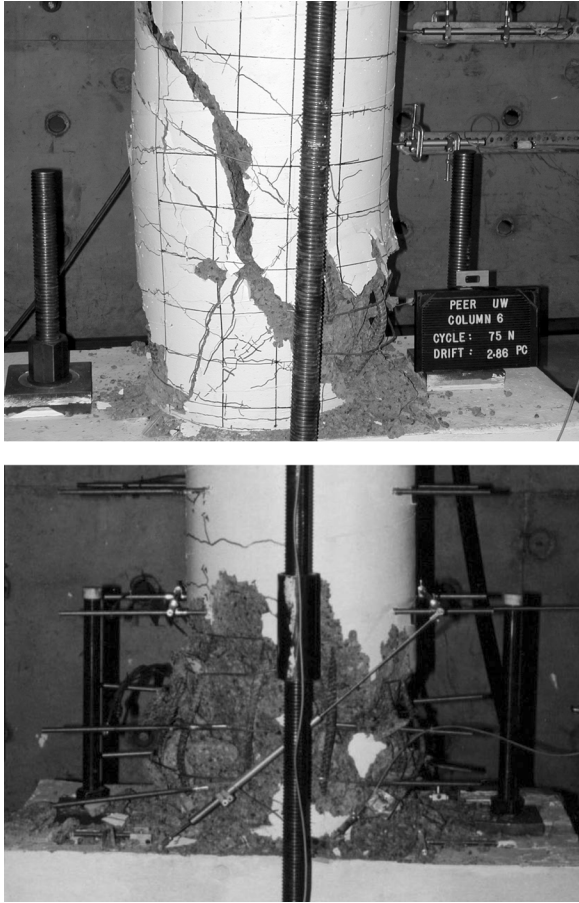
Figure 8 – Examples of: (a) flexure-shear failure; and (b) axial-flexure failure.